Laser–Tissue Interaction During Transmyocardial Laser Revascularization

E. Duco Jansen, PhD, Martin Frenz, PhD, Kamuran A. Kadipasaoglu, PhD, T. Joshua Pfefer, MS, Hans J. Altermatt, MD, Massoud Motamedi, PhD, and Ashley J. Welch, PhD

Biomedical Engineering Program, University of Texas at Austin, Texas Heart Institute, Houston and Biomedical Laser and Spectroscopy Laboratory, University of Texas Medical Branch, Galveston, Texas; and Institute of Applied Physics and Pathological Institute, University of Bern, Bern, Switzerland

Background. **The clinical procedure known as transmyocardial revascularization has recently seen its renaissance. Despite the promising preliminary clinical results, the associated mechanisms are subject to much discussion. This study is an attempt to unravel the basics of the interaction between 800-W CO_2 laser radiation and biological tissue.**

Methods. **Time-resolved flash photography was used to visualize the laser-induced channel formation in water and in vitro porcine myocardium. In addition, laser-induced pressures were measured. Light microscopy and birefringence microscopy were used to assess the histologic characteristics of laser-induced thermal damage.**

Results. **The channel depth increased logarithmically with time (ie, with pulse duration) in water and porcine myocardium. Pressure measurements showed the occurrence of numerous small transients during the laser pulse, which corresponded with channel formation, as well as local and partial channel collapse during the laser pulse. Twenty millimeters of myocardium was perforated in 25 ms. Increasing the pulse duration had a small effect on the maximum transversable thickness, but histologic analysis showed that thermal damage around the crater increased with increasing pulse duration.**

Conclusions. **Several basic aspects of the interaction of high-power CO_2 laser radiation with myocardial tissue and tissue phantoms were studied in vitro. Although the goal of this study was not to unravel the mechanisms responsible for the beneficial effects of transmyocardial revascularization, it provided important information on the process of channel formation and collapse and tissue damage.**

(Ann Thorac Surg 1997;63:640–7)
© 1997 by The Society of Thoracic Surgeons

Despite major research efforts, coronary artery disease remains the leading cause of death in the Western world. Although procedures such as percutaneous transluminal coronary angioplasty and coronary artery bypass grafting are proven methods of treating ischemic heart disease, many patients have conditions, in particular distal or diffuse coronary artery disease, that are not amenable to these therapies.

After Sen and colleagues [1] in 1965 reported the creation of multiple transmyocardial puncture tracts as an effective new way to revascularize the myocardium, Mirhoseini and Cayton [2] were the first to propose using a laser to drill transmyocardial channels to convey oxygen-rich blood directly from the left ventricular cavity to the myocardium.

Since then, many groups have conducted experiments using a variety of lasers, irradiation conditions, and animal models to explore this possibility [3–12]. Recently, with the availability of a clinical, high-power (800-W) CO_2 laser, it became possible to perform this procedure on a beating heart. The myocardium can be traversed in one laser pulse during a fraction of one cardiac cycle. The preclinical and clinical results have been promising [13], and clinical trials are currently under way [14–18]. Nevertheless, the mechanism of action of this laser procedure remains largely undefined. It is not clear, for instance, whether laser-induced channels remain open for prolonged times or whether the beneficial effects of the procedure stem from the channels created or from a subsidiary adaptation elicited by other components of the laser-induced insult [9]. Several mechanisms have been hypothesized by a number of researchers, ranging from a placebolike effect to laser injury–induced changes in the mechanical compliance of the myocardium and from a laser-induced triggering of neovascularization to a laser-induced inhibition of pain, which allows exercise-induced neovascularization (cardiac rehabilitation) to be accomplished. Thus far, much of the disagreement between study findings can be attributed to the lack of a consistent and appropriate animal model that accurately simulates the compromised, ischemic, preconditioned human myocardium.

Because of the renewed interest in the application of lasers in cardiothoracic surgery driven by transmyocardial laser revascularization (TMLR), and to fully appreciate the effects of laser radiation on tissue, in particular myocardial tissue, we will briefly review a few of the

Accepted for publication Sep 23, 1996.

Address reprint requests to Dr Jansen, Department of Biomedical Engineering, Box 1631, Station B, Vanderbilt University, Nashville, TN 37203 (e-mail: duco@vuse.vanderbilt.edu).

© 1997 by The Society of Thoracic Surgeons
Published by Elsevier Science Inc

0003-4975/97/$17.00
PII S0003-4975(96)01143-5

basic concepts of laser–tissue interaction. For an extensive review we refer readers to the articles by Welch [19] and Jacques [20]. The most important property of the laser radiation is the wavelength, because it determines how strongly the laser radiation is absorbed and scattered in the irradiated media. For efficient ablation it is desirable to have strong absorption of the laser radiation so that the optical energy which is converted to heat upon absorption is confined to a relatively small volume. Tissue contains several endogenous chromophores, such as hemoglobin, proteins, and water, which all absorb light in different parts of the spectrum. For near- and far-infrared laser radiation (as generated by holmium, erbium, and CO_2 lasers), the most important chromophore is tissue water, which is present in abundance (~80%) in soft biologic tissue. A measure of absorption is the penetration depth (δ [μm]), which is the distance in the absorbing medium it takes for the fluence (W/m^2) of the laser beam to be reduced to 1/e (~37%) of the incident irradiance at the surface. Light absorption is also quantified by the absorption coefficient ($\mu_a[mm^{-1}]$), where $\delta = 1/\mu_a$. For the CO_2 laser, which emits radiation with a wavelength of 10.6 μm, the absorption coefficient in soft tissue (such as myocardium) is approximately 80 mm^{-1}, which corresponds to a penetration depth of 12.5 μm [21].

There are two types of lasers: continuous-wave and pulsed. An example of a pulsed laser is the pulsed holmium:yttrium-aluminum-garnet laser, which, in the free-running mode, has a pulse duration of 250 μs; it has been suggested as another candidate for performing TMLR [9, 22]. The parameters defined for a pulsed laser are the pulse duration (s), pulse energy (mJ), the average power (total energy/unit time), the peak power (pulse energy/pulse duration), and the radiant exposure, also known as fluence (pulse energy/unit area). The clinically used CO_2 laser, on the other hand, is a continuous-wave laser. Parameters of importance for continuous-wave lasers are power (total energy/unit time), irradiance (power/unit area), and the duration of laser exposure (time the laser is emitting radiation). For the study at hand, it is important to bear in mind that, at a constant power, the amount of energy delivered per unit of time is constant, whereas the total amount of energy is directly proportional to the duration of exposure. A summary of this nomenclature is provided in Table 1.

Table 1. Laser Terminology

Term	Symbol	Units	Description
Wavelength	λ	m	"Color" of the light
Penetration depth	δ	m	Depth in medium where the fluence is reduced to 1/e (37%) of the incident value at the surface
Absorption coefficient	μ_a	1/m	Measure for the probability that a photon will be absorbed, per definition $\mu_a = 1/\delta$
Pulse duration	τ_p	s	Duration of laser emission
Pulse energy	E_p	J	Amount of energy in one laser pulse
Average power	W_{avg}	W (J/s)	Total amount of energy per second
Peak power	W_{peak}	W (J/s)	Total amount of energy in the laser pulse divided by the pulse duration (ie, the average power during the pulse)
Radiant exposure (fluence)	H	J/m^2	Amount of energy delivered to sample surface per unit area (for pulsed lasers)
Irradiance	I	W/m^2	Power per unit area (for continuous-wave lasers)

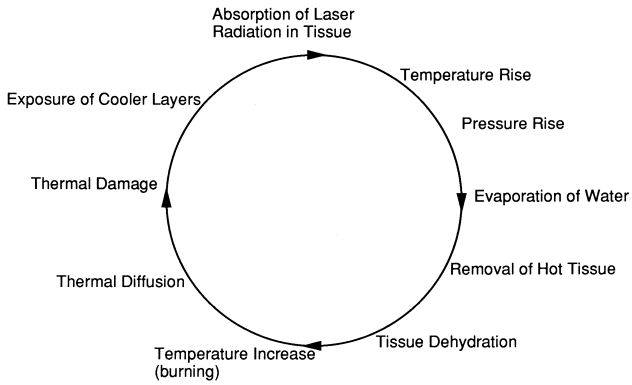


Fig 1. Chronology of the events associated with continuous-wave laser ablation of soft tissue.

The chronology of the events that occur during the continuous-wave ablation of soft tissue has been fairly well documented and in essence follows that shown in the schematic in Figure 1. Upon absorption of laser radiation by tissue water, rapid heating occurs. As energy is spent on vaporization (latent heat), the temperature ranges from 100° to 150°C. After local desiccation of the tissue, the temperature continues to increase to 350° to 450°C, at which point carbonization and ablation (removal) take place, thus exposing new cooler layers. This process continues as the ablation front moves deeper into the tissue. Although the CO_2 laser has been used in many medical specialties since the early days of laser medicine, as evidenced by the numerous published reports of studies on this subject, thus far treatment has involved laser powers of typically no more than 80 W. Transmyocardial laser revascularization represents the first clinical application of a high-power CO_2 laser source similar to the ones used in material processing (large-scale cutting and welding of metals).

The goal of this study was to investigate the basic mechanisms of the interaction of high-power CO_2 laser radiation with soft tissue as it is used in TMLR. The experiments were designed to visualize and determine the characteristics of the ablation process using this laser.

Material and Methods

An 800-W CO_2 laser (The Heart Laser; Laser Engineering, Inc [PLC], Milford, MA) was used in this study. This

clinical laser, which is designed especially for TMLR, is equipped with an articulated arm and an endpiece with a 150-mm focal-length lens which focuses the laser beam to a spot size of approximately 1 mm in diameter at the tissue surface. The laser power is fixed at 800 W of continuous CO_2 laser radiation (λ = 10.6 μm). The laser emits a single burst of energy with a pulse duration that can be varied from 10 to 99 ms (corresponding to total energies of from 8 to 79.2 J). In the clinic, the laser is synchronized to the electrocardiogram of the patient and triggered at a variable delay time after the R wave of the electrocardiogram, whereas in our experiments an electrocardiographic simulator was used to trigger and synchronize the laser. For all tissue experiments, the tissue sample was suspended in a basin filled with water, such that the bottom was under water and the top was not submerged but kept moist.

Channels in Water

Carbon dioxide laser radiation (λ = 10.6 μm) is strongly absorbed in water, which is the main constituent of soft tissue. To visualize the ablation process in water, a standard time-resolved flash photography setup was used in the shadow mode (Fig 2). The electrocardiographic simulator used to trigger the CO_2 laser was also used to trigger a delay generator (DGD-535; Stanford Research Systems, Sunnyvale, CA), which triggered a strobe light. Images of the growing channel were recorded using a CCD (video) camera and stored on videotape. The sequence of events was reconstructed by varying the delay time between the start of the laser pulse and the strobe light. The images were used to measure the bubble size and shape as a function of time after the start of the laser pulse. In addition, a needle hydrophone (Imotec, Würselen, Germany) was used to document the presence of any laser-induced pressure transients. Because the pressure transients were found to be fairly weak, an amplifier with a fast time response (100 MHz) was used. The amplified pressure signals were displayed and stored on a digital storage oscilloscope (TDS 520A; Tektronix, Wilsonville, OR).

Tissue Experiments

Fresh porcine myocardium was obtained from a local slaughterhouse. The hearts were stored at 4°C wrapped in plastic to prevent desiccation until the moment of use (<24 hours postmortem). Samples of tissue (2 × 4 cm) were cut from the hearts and suspended in the water bath so that the top surface (epicardial side) was several mm above the water level. Time-resolved flash photography was used to image the bottom surface of the tissue during delivery of the laser pulse.

The following experiment was designed to determine the channel depth as a function of time. The CO_2 laser was equipped with a continuous-wave helium-neon (He-Ne; λ = 632 nm) aiming beam, which was coaligned with the CO_2 laser beam and therefore also delivered through the articulated arm. A photodiode was placed underneath the water bath in which a slab of tissue was mounted, and the signal from the photodiode was recorded on a digital storage oscilloscope (see Fig 2). As the

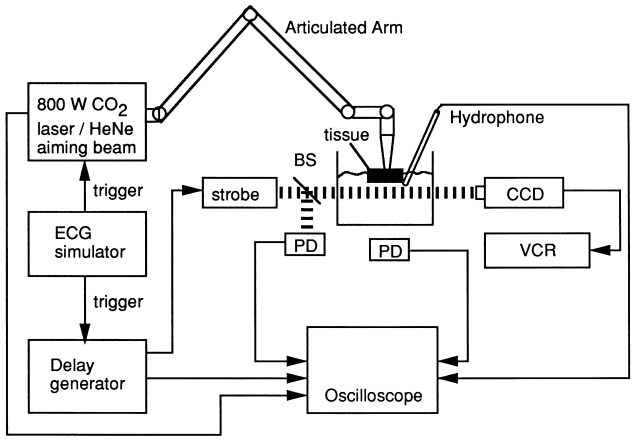


Fig 2. The experimental setup used to take the time-resolved, fast flash images of the ablation-associated events in a transparent medium (water or tissue phantom gels). For tissue burn-through studies, the helium-neon (HeNe) *aiming beam, which is coaligned with the CO_2 beam, is detected by a photodetector* (PD) *underneath the water bath. As the channel is formed, the remaining thickness of the tissue decreases and thus the transmitted He-Ne signal increases.* (BS = *beam splitter;* CCD = *charge-coupled device [video camera];* ECG = *electrocardiographic;* VCR = *video cassette recorder.)*

CO_2 laser beam drilled a channel through the tissue, the thickness of the remaining tissue decreased until ultimately total penetration was achieved. Consequently, the amount of He-Ne laser radiation reaching the photodiode underneath the tissue increased with the decreasing tissue thickness and was used to determine the moment of total tissue penetration (because the He-Ne wavelength is highly scattered in tissue but is transmitted through the water underneath the tissue). Afterward, the thickness of the tissue slab at each channel site was determined using a needle with millimeter markings on it.

In addition, several tissue samples were irradiated with 10-, 30-, 40-, and 50-ms-long laser pulses ($n \geq 3$ for each irradiation condition). These samples were fixed in 10% buffered formalin and saved for histologic analysis. The tissue samples were embedded in paraffin, and sections were cut at the epicardial side, in the middle of the sample, and at the endocardial side. Sections were stained using the standard hematoxylin and eosin staining technique and evaluated for tissue damage adjacent to the laser-induced crater using light microscopy and polarization (birefringence) microscopy.

Results

Figure 3 shows the sequence of events occurring during delivery of a 10-ms, 800-W (ie, 8 J) CO_2 laser pulse just below the surface of the water bath at room temperature. It can be seen that the laser radiation rapidly vaporized a channel to a depth of about 12 mm. The approximate diameter of the channel was 1 mm, which corresponded to the diameter of the laser beam. The cylindrically shaped channel lengthened as laser radiation was continuously deposited through the enlarging vapor cavity, because water vapor is much less absorbing than liquid

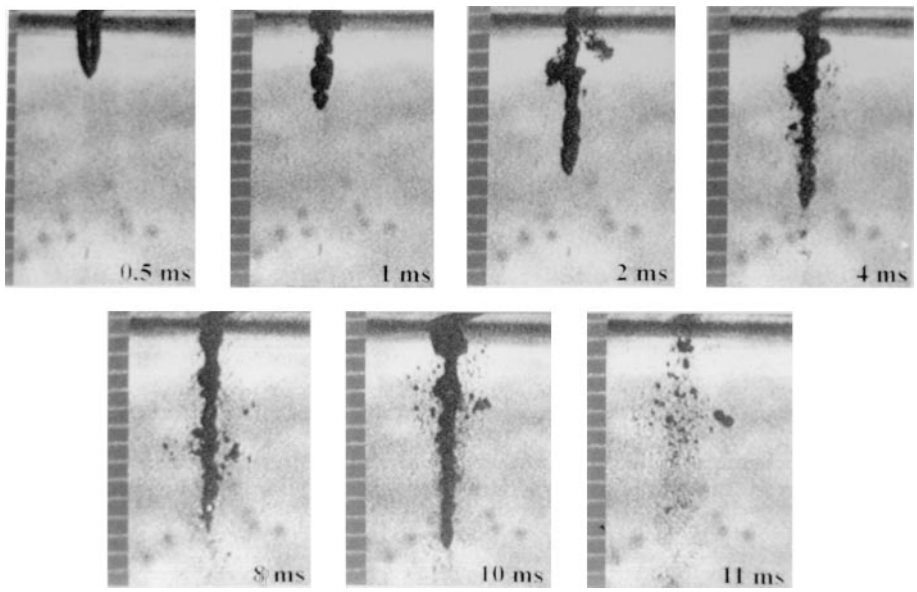


Fig 3. Sequence of images taken during the irradiation of water with the 800-W CO_2 laser. Pulse duration was 10 ms (8 J), and the spot size at the surface was 1 mm in diameter. The delay times with respect to the start of the laser pulse are shown in the lower righthand corner. The scale in the images is a millimeter scale.

water at this wavelength [21]. Immediately after the end of the laser pulse, the channel disappeared as the water vapor condensed at the channel wall and remaining vapor pockets and convective flows of heated water are visible (Fig 3, last frame). All bubbles disappeared within a few milliseconds, and no lasting bubbles were observed.

Figure 4 shows the length of the vapor bubble as a function of time as it was measured from images such as those in Figure 3. The average is shown in the graph, with the error bar representing the standard deviation (n = 20). It appeared that, after the initial rapid growth, the channel deepened logarithmically with time. This experiment was performed using laser pulse durations of 10, 30, 50, and 70 ms. As expected, the channel length at any given time was not a function of the ultimate duration of the laser pulse, because the power was constant. Naturally, longer pulse durations maintained a growing channel for the duration of the laser pulse, ie, the channel collapsed immediately after the end of the laser pulse. Therefore, all data points from all four pulse durations were averaged when appropriate (ie, while the laser was on).

A typical example of a pressure measurement with the hydrophone for a 40-ms pulse is shown in Figure 5. With the hydrophone placed 12 mm below the water surface and 3 mm from the center of the He-Ne aiming beam, multiple pressure peaks were observed to occur in a more-or-less random fashion. The maximum pressure peak detected by the amplified hydrophone had an amplitude of only 0.12 bar.

A typical trace of the photodetector collecting He-Ne laser light during CO_2 laser–induced channel formation in myocardium is shown in Figure 6A (the actual 40-ms-long CO_2 laser pulse is shown as a reference in Figure 6B). The moment of tissue penetration was derived from

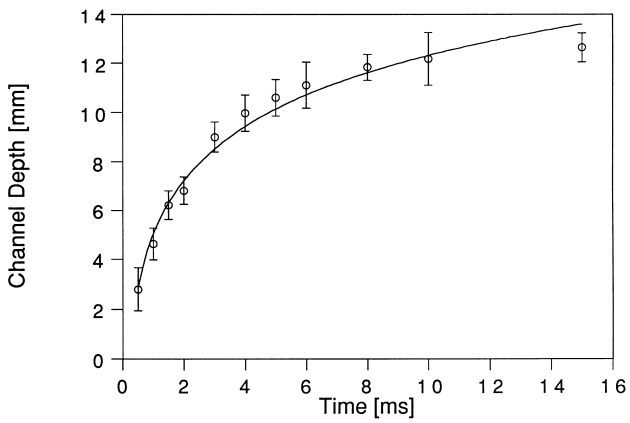


Fig 4. Length of the vapor channel in water as a function of time. The measurements were taken from images like those in Figure 3. Pulse durations were 10, 30, 50, and 70 ms, but no differences in channel length at any time were seen for the different pulse durations. Shown are the average channel length and standard deviation (n = 20). The line represents a logarithmic fit to the data (r = 0.98).

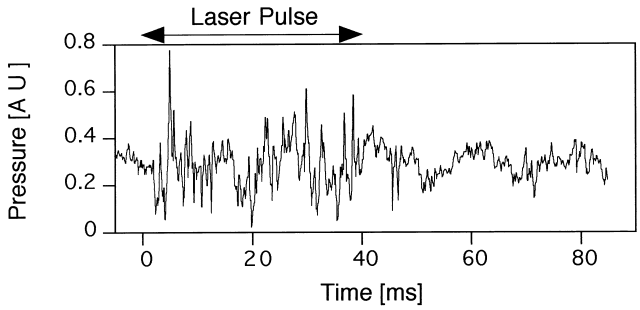


Fig 5. Hydrophone trace measured during a 40-ms CO_2 laser pulse in water. The CO_2 laser pulse is indicated by the horizontal line. The hydrophone was positioned with the tip 12 mm in the water and 3 mm away from the center of the laser beam. The signal was amplified 200 times, causing it to be quite noisy. However, it can be seen that pressure transients occurred during the laser pulse. The maximum absolute pressure at the sensor corresponded to 0.12 bar. (AU = arbitrary units.)

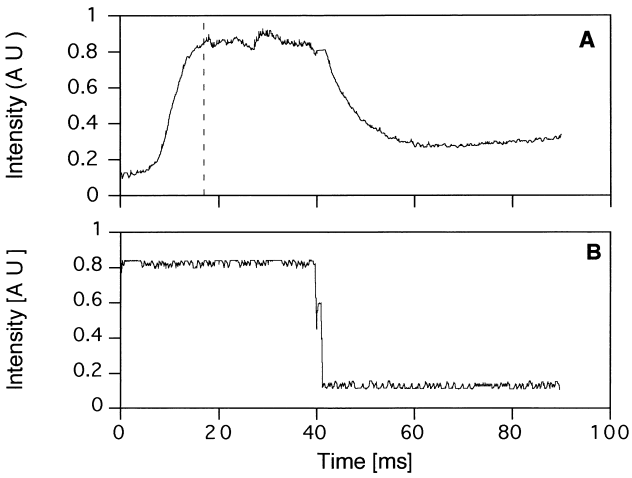


Fig 6. The trace of the photodiode-collecting helium-neon laser light at the bottom of a tissue slab (porcine myocardium) with a thickness of 20.5 mm (A). Also shown is the trace from the 40-ms CO_2 laser pulse (B). The CO_2 laser was coaligned with the helium-neon laser (aiming beam) and ablated the tissue, causing an increase in helium-neon light transmission. The time to penetration was 17.5 ms. (AU = arbitrary units.)

the He-Ne signal, which yielded the time it took the CO_2 laser to produce an ablation crater that traversed the thickness of the myocardium. The time of penetration was defined as the time the He-Ne signal reached 95% of its maximum value and is indicated in Figure 6A. For the sample shown in Figure 6A, the penetration time was 17 ms (tissue thickness was approximately 20.5 mm). After the end of the laser exposure (ie, after 40 ms in Figure 6A), the He-Ne transmission decreased again over the next 20 ms. This is an indication that the channel closes immediately after the end of the laser exposure. The transmission of the He-Ne light does not reach its original baseline value for seconds because of scattering of the light in the water underneath the fluid caused by ejected debris and small bubbles in the water. Figure 7 shows the relationship between the thickness of the ablated crater and the time needed to ablate all the way through. Again, the relationship between the time and channel depth (ie, tissue thickness) was logarithmic. The fitted curve in water from Figure 4 is also plotted as a reference.

In a separate experiment, the time-resolved photography setup was used to image the bottom of a tissue sample during the laser pulse. To do this, a slab of tissue that was approximately 10 mm thick was used. From the curve in Figure 7, it was known that it takes approximately 7 ms to drill through a 10-mm-thick slab of tissue. Thus the flash delay was set at 7 ms. It was observed that immediately after the laser beam ablated the 10-mm-thick tissue (ie, after 6–7 ms), the channel continued to lengthen in the water underneath the tissue (Fig 8). However, within milliseconds the channel in the water disappeared and a cloud of steam and particles was seen, which was ejected out of the bottom of the crater in the tissue into the liquid below (Fig 8D). During the remainder of the laser pulse, the laser radiation maintained an open channel in the tissue (which was shown in the He-Ne experiment) but no channel was formed in the water underneath the tissue.

Typical histologic cross-sections of CO_2 laser–induced craters in porcine myocardium in vitro are shown in Figure 9. The crater on the left (Figs 9a, 9b) was made with a 50-ms (40-J) laser pulse, and the crater on the right (Figs 9c, 9d) was made with a 10-ms (8-J) laser pulse. The sections shown were obtained close to the epicardial side of the myocardium, which is the side from which the tissue was irradiated. For both pulse durations, regular light microscopy revealed the presence of a fairly regular crater with a diameter of approximately 500 μm and a zone of thermal damage of approximately 150 μm (50 ms) and 50 μm (10 ms), indicated by discoloration and vacuolization. Considerably more vacuolization was present around the channel made with the 50-ms laser pulse than around the channel made with the 10-ms laser pulse. Birefringence microscopy, however, revealed the existence of a much larger zone of thermally altered tissue. A significant difference was observed between the damage along the myofibrils and the damage across the myofibrils. The damage in the direction across the fibers was approximately 300 μm (50 ms) and 100 μm (10 ms), whereas the extent of damage along the fibers was 650 μm (50 ms) and 550 μm (10 ms). The thermal damage along the fibers strongly depended on the amount of tissue tearing that had taken place. It was observed that, along the myofibrils, tissue layers were separated over a distance of up to 2 mm beyond the crater.

Comment

Several aspects of the interaction of high-power (800-W) CO_2 laser radiation, as it is used in TMLR, with soft biologic tissue have been investigated. Carbon dioxide laser radiation ($\lambda = 10.6$ μm) is highly absorbed by water, which, as noted previously, is abundant in soft biologic tissue such as myocardium ($\mu_a = 80$ mm^{-1}; penetration

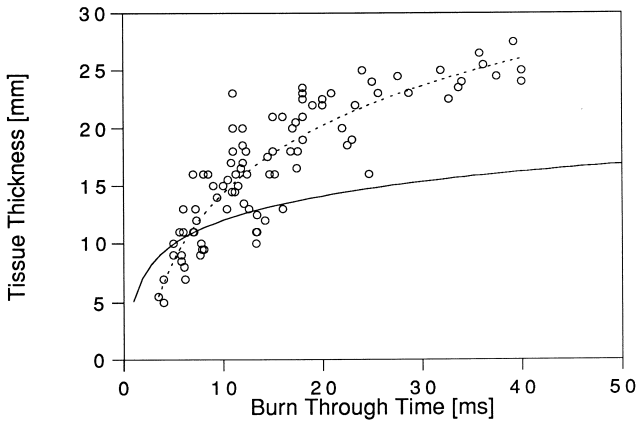


Fig 7. Tissue thickness (porcine myocardium) as a function of the time needed to ablate a channel all the way through the tissue. The burn-through time was determined from the helium-neon traces shown in Figure 6. Also shown is the fitted curve of the channel depth versus time in water from Figure 4.

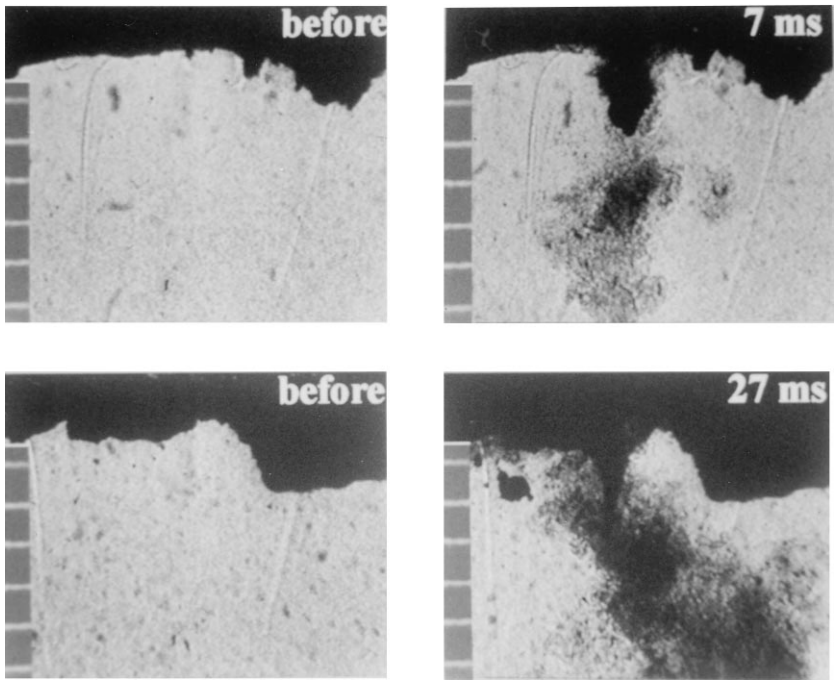


Fig 8. Time-resolved photographs of the bottom of a 10-mm-thick slab of porcine myocardium in water. The dark areas on the top are the bottom of the tissue (silhouette). The images on the left are control pictures taken before the laser pulse. The images on the right were obtained just after total tissue penetration was achieved at 7 ms after the start of the 40-ms laser pulse (top) and 20 ms after total tissue penetration (ie, 27 ms after the start of the 40-ms laser pulse) (bottom). The scale represents a millimeter scale.

depth = 12.5 μm) [21]. Therefore the radiation is absorbed in a small volume, making this laser a legitimate candidate for efficient ablation.

Channel Formation

Upon irradiation of the water surface, the laser radiation is absorbed and causes rapid heating and subsequent vaporization of the liquid once sufficient energy has been deposited. Hence a moving ablation front is formed during the laser pulse (see Fig 1). It should be realized that, upon the phase transition from liquid water to water vapor, a significant volumetric expansion takes place (the volumetric expansion factor is 1,620 for water at 1 atm). It is expected that this volumetric expansion helps open a vapor channel in the liquid. From the images observed in water (see Fig 3), it is evident that the laser radiation forms a channel that initially deepens rapidly, at a velocity of approximately 6 mm/ms. The initial rapid growth rate slows considerably as the channel becomes longer because the channel tends to collapse locally and a greater portion of the laser radiation is then used to maintain the open channel (see Fig 4). It is expected that this local collapse is caused by a combination of the condensation of water vapor at the channel wall and hydrostatic and surface tension forces. This dynamic channel behavior is supported by the pressure measurements shown in Figure 5. The small pressure transients are caused by the ablation process (explosive vaporization) that is maintained for the duration of the laser pulse, leading to the irregular shape of the channel (see Fig 3). The partial closure of the vapor channel at different places during the laser pulse may also contribute to the observed pressure signal. The local collapses of the channel can also be observed in Figure 3 as invaginations in the channel at various depths. However, the recorded pressures were very weak (maximum pressure measured is 0.12 bar) and had to be amplified (gain = 200), causing the signal to become fairly noisy. This indicates that the biologic mechanism responsible for the clinical outcome of TMLR using the CO_2 laser is unlikely to be associated with laser-induced pressure effects.

During the ablation of myocardium, which was monitored using the coaligned He-Ne laser, it was observed that the He-Ne signal increased as soon as ablation of the tissue started (ie, the effective thickness of the tissue decreased). This continued until the moment of total tissue penetration, at which time the CO_2 laser had ablated a hole all the way through the myocardium. At this time the He-Ne signal became more-or-less stable, though somewhat noisy, because a cloud of steam and ablation debris was ejected from the bottom of the tissue (see Fig 8), causing the He-Ne laser light to scatter. After the end of the CO_2 laser pulse, the channel collapsed within 20 ms, as shown by a rapid drop in the He-Ne light transmitted. However, in contrast to the clinical situation in which a dynamic gradient between the intraventricular and intramyocardial pressure is present that may stimulate flow and that could help maintain an open channel, no pressure gradient is present under the in vitro experimental conditions, and this may be responsible for this rapid channel collapse. As the steam cloud and ejected particles dissipated and diffused, the He-Ne signal slowly decreased back to the original baseline value over a period of seconds (not shown). Using the moment of total penetration from the He-Ne signal for different myocardial thicknesses, we were able to reconstruct a channel depth–versus–time graph, thus somewhat compensating for our inability to obtain images inside the opaque tissue. As the channel in tissue became deeper, more laser energy was needed to maintain an

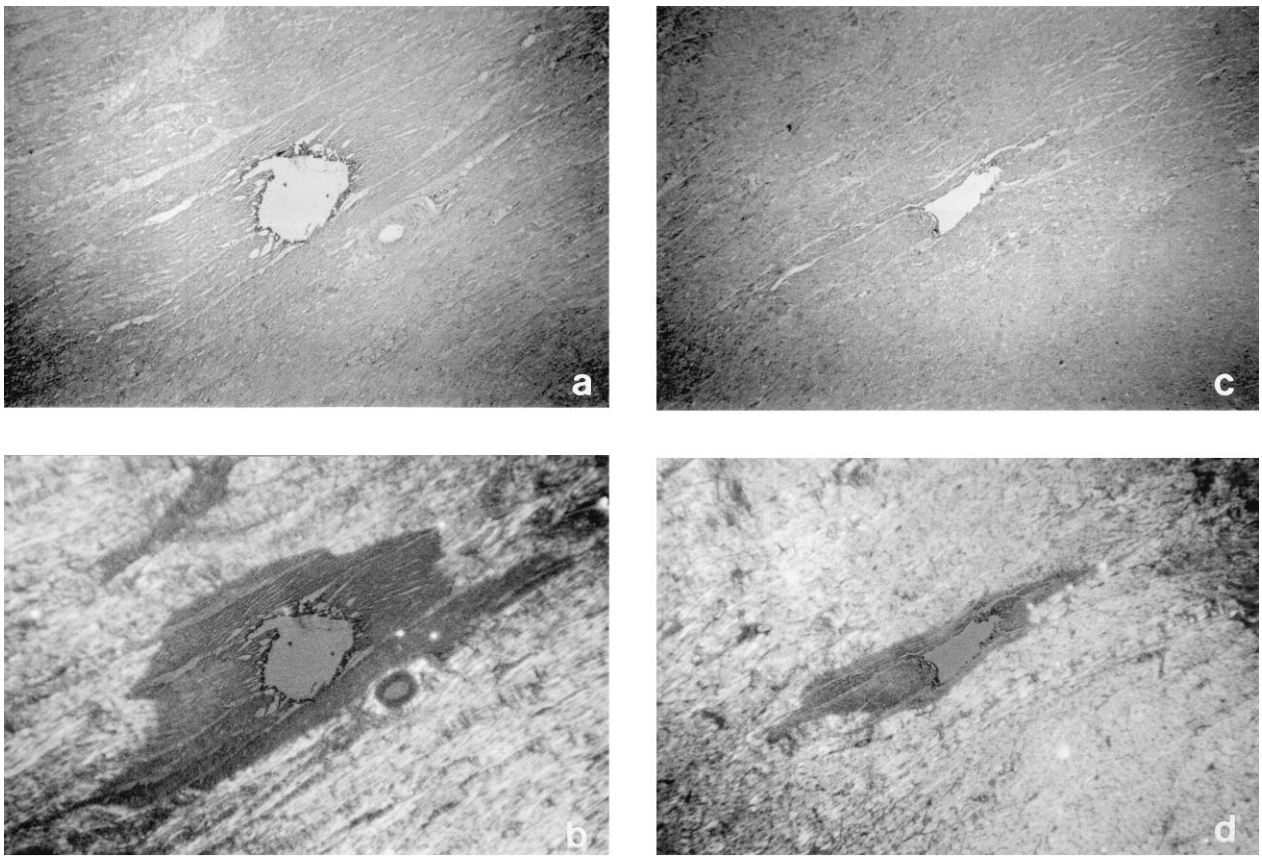


Fig 9. Histologic cross-sections of porcine myocardium irradiated in vitro with an 800-W CO_2 laser. The tissue was irradiated from the epicardial side, and the sections were taken close to the surface. (a, b) Pulse duration of 50 ms (40 J). (c, d) pulse duration of 10 ms (8 J). a and c are the standard light microscopic images and b and d are the birefringence images.

open channel and to negate the forces driving the channel collapse. Consequently, the channel depth increased logarithmically with time and the maximum channel depth reached a plateau. The maximum depth of the channel depended on the medium and was less in water than in tissue.

A surprising finding of this study was the lack of channel formation in the fluid below the myocardium. Although channel formation through the solid produced a cloud of steam and ejected particles at the bottom of the solid, there was no evidence of a channel in the fluid. While performing several experiments to confirm this unexpected finding, it was also found that (1) when a fluid overlies the solid, the channel propagates through the fluid and ablates a channel in the solid and (2) when blood is used as the liquid, results are obtained similar to those in water, indicating that the observation is not a water-related artifact. In practical terms, this means that the blood inside the heart may act as an effective "beam stop" once the entire ventricular wall is traversed. The steam and particle cloud observed corresponds to the cloud seen clinically during transesophageal echocardiography.

Tissue Damage

Considerable zones of thermal damage were created adjacent to the crater (see Fig 9). Although this was not visible on regular (hematoxylin and eosin) light microscopy studies, birefringence microscopy visualized the true extent of the thermally altered tissue. This polarization microscopic technique is based on the fact that structured and well-organized fibrillar tissues such as collagen and actin-myosin fibers have the ability to rotate the polarization angle of linearly polarized light (a property called birefringence) [23]. Upon denaturation, the tissue loses this property, causing it to be expressed as a dark area on the image. Although denaturation (and thus birefringence loss) depends not only on the tissue temperature but also on the time the tissue remains at that temperature (ie, it is a rate process), typically birefringence loss is associated with an absolute temperature of approximately 55° to 60°C [23]. The finding that the observed zone of thermal damage at the epicardial side is considerably larger after a 50-ms laser pulse than after a 10-ms laser pulse can be explained by the fact that, in addition to reaching a higher temperature, the tissue is exposed to this temperature for a longer time. This allows more heat to diffuse out of the directly irradiated volume toward cooler, adjacent tissue. Additionally, the prolonged exposure contributes to the denaturation process itself, because, as mentioned before, both time and temperature govern thermal denaturation.

The asymmetric distribution of thermal damage which can be seen as a more extensive zone of thermally altered

tissue coaxial with the direction of myofibrils (ie, along the fibers) as compared with the zone of thermal damage perpendicular to the direction of the myofibrils (ie, across the fibers) was attributed to the more efficient diffusion of heat in this direction [24]. In addition, the pressurized volume of ablation products causes tearing of tissue. Because the hot steam under pressure will take the path of least resistance, tearing occurs along the fibers. This should come as no surprise, because it is easier to separate myofibrils from each other than to break them using tensile force. The fact that the fissures seen on histologic studies have a zone of thermally altered tissue around them indicates the presence of hot steam and ablation products during the irradiation.

The main limitation of this study is the fact that this is an in vitro study. Hence the results should be extrapolated carefully to the clinical situation in which living, perfused myocardium is treated. The physical mechanisms associated with the ablation of myocardial tissue and the trends described here are expected to be the same in vivo, but the exact numbers (eg, extent of thermal damage, time needed to establish a transmural channel) may differ slightly.

Conclusion

In conclusion, the primary finding of this study is that, because the left ventricular myocardium in human beings is typically not more than 20 mm thick, it seems that a pulse duration of 25 ms would be sufficient to traverse the myocardium under the in vitro experimental conditions used in this study. Increasing the pulse duration only has a marginal effect in terms of being able to traverse thicker pieces of myocardium, and this occurs at the expense of increased thermal damage. Second, ablation-induced pressure waves were found to be of insignificantly small amplitude. Therefore it is unlikely that the beneficial effects of CO_2 laser–assisted TMLR result from laser-induced pressure transients. Third, under the experimental conditions in which a pressure gradient is absent, the laser-induced channel collapsed or closed within tens of milliseconds.

Whether the extent of thermal damage or laser-induced mechanical tissue tearing has a positive or negative effect on the clinical outcome of TMLR is still unknown.

This work was supported in part by the Albert and Clemmie Caster Foundation and The Office of Naval Research (grant no. N00014-91-J1564). Martin Frenz thanks the German Science Foundation (grant Fr 1147/1-1) for their financial support during his research fellowship at The University of Texas at Austin. We thank Dr John Pearce for use of his birefringence microscope.

References

1. Sen PK, Udwadia TE, Kinare SG, Parulkar GB. Transmyocardial revascularization: a new approach to myocardial revascularization. J Thorac Cardiovasc Surg 1965;50:181–9.
2. Mirhoseini M, Cayton MM. Revascularization of the heart by laser. J Microsurg 1981;2:253–60.
3. Horvath KA, Smith WJ, Laurence RG, Schoen FJ, Appleyard RF, Cohn LH. Recovery and viability of an acute myocardial infarct after transmyocardial laser revascularization. J Am Coll Cardiol 1995;25:258–63.
4. Hardy RI, James FW, Millard RW, Kaplan S. Regional myocardial blood flow and cardiac mechanics in dog hearts with CO_2 laser-induced intramyocardial revascularization. Basic Res Cardiol 1990;85:179–97.
5. Okada M, Shimizu K, Ikuta H, Horii H, Nakamura K. A new method of myocardial revascularization by laser. Thorac Cardiovasc Surg 1991;39:1–4.
6. Landreneau R, Nawarawong W, Laughlin H, et al. Direct CO_2 laser revascularization of the myocardium. Lasers Surg Med 1991;11:32–45.
7. Jeevanandam V, Auteri JS, Oz MC, Watkins JF, Rose E, Smith CR. Myocardial revascularization by laser induced channels. Surg Forum 1991;41:225–7.
8. Whittaker P, Kloner RA, Przyklenk K. Laser-mediated transmural myocardial channels do not salvage acutely ischemic myocardium. J Am Coll Cardiol 1993;22:302–9.
9. Whittaker P, Rakusan K, Kloner RA. Transmural channels can protect ischemic tissue: assessment of long-term myocardial response to laser- and needle-made channels. Circulation 1996;93:143–52.
10. Zheng SM, Kloner RA, Whittaker P. Ablation and coagulation of myocardial tissue by means of a pulsed holmium: YAG laser. Am Heart J 1993;126:1474–7.
11. Kohmoto T, Fisher PE, Anguo G, Zhu SM, Smith CR, Burkhoff D. Does blood flow through transmyocardial CO_2 laser channels. J Am Coll Cardiol 1996;27(Suppl A):13A.
12. Whittaker P, Kloner RA. Excimer laser channels protect against myocardial ischemia. J Am Coll Cardiol 1996; 27(Suppl A):13A.
13. Cooley DA, Frazier OH, Kadipasaoglu K, Pehlivanoglu S, Shannon RL, Angelini P. Transmyocardial laser revascularization: anatomic evidence of long-term channel patency. Texas Heart Inst J 1994;21:220–4.
14. Crew JR, Thuener M, Jones R, Ryan C, Chimenti C, Fisher JC. Transmyocardial revascularization. J Am Coll Cardiol 1994;23(Suppl):151A.
15. Mirhoseini M, Cayton MM, Shelgikar S. Transmyocardial laser revascularization. J Am Coll Cardiol 1994;23(Suppl):416A.
16. Kakavas PW, March RJ, Macioch JE, et al. Effects of transmyocardial laser revascularization on regional left ventricular function and contractile reserve: evaluation by resting and dobutamine stress echocardiography. Circulation 1995;92(Suppl 1):176.
17. Frazier OH, Cooley DA, Kadipasaoglu KA, et al. Myocardial revascularization with laser: preliminary findings. Circulation 1995;92(Suppl 2):58–65.
18. Cooley DA, Frazier OH, Kadipasaoglu KA, et al. Transmyocardial laser revascularization: clinical experience with twelve-month follow-up. J Thorac Cardiovasc Surg 1996;111:791–9.
19. Welch AJ, Torres JH, Cheong WF. Laser physics and laser-tissue interaction. Texas Heart Inst J 1989;16:141–9.
20. Jacques SL. Laser-tissue interactions: photochemical, photothermal and photomechanical. Surg Clin North Am 1992;72: 531–58.
21. Irvine WM, Pollack JB. Infrared optical properties of water and ice spheres. Icarus 1968;8:324–60.
22. Oesterle SN, Walton AJ, Kernoff R, et al. Percutaneous trans-endocardial laser revascularization. Circulation 1995; 92(Suppl 1):616.
23. Thomsen SL, Pearce JA, Cheong WF. Changes in birefringence as markers of thermal damage in tissues. IEEE Trans Biomed Eng 1989;53:1174–9.
24. Lentz CP. Thermal conductivity of meats, fats, gelatin gels and ice. Food Technol 1961;14:243–7.